CHARACTERIZING ELECTRICAL INTERACTIONS OF TISSUE WITH TIME-VARYING GRADIENT FIELDS: SIMULATIONS AND MEASUREMENTS

Stefano Mandija[1], Astrid L.H.M.W. van Lier[1], Axel Thielscher[2,3], Andre Antunes[4], Sebastiaan F.W. Neggers[5], Peter R. Luijten[1], and Cornelis A.T. van den Berg[1]
[1]Imaging Division, University Medical Center, Utrecht, Netherlands, [2]Danish Research Centre for Magnetic Resonance, Copenhagen, Denmark, [3]Technical University of Denmark, Kgs. Lyngby, Denmark, [4]Max Planck Institute for Biological Cybernetics, Tübingen, Germany, [5]Rudolf Magnus Institute of Neuroscience, University Medical Center, Utrecht, Netherlands

Introduction: Knowledge on the relation between the electrical conduction at low frequency (Hz-kHz) and in-vivo tissue composition and structure is currently limited. Research on ex-vivo tissues demonstrated that in this frequency range the human body is electrically very heterogeneous (Fig.1)[1]: biological structures such as cell membranes and neurons constitute strong electrical impedance variations that affect current flow. Having reliable information on in-vivo tissue conductivity is important for various purposes, e.g. to calculate the induced currents in transcranial magnetic stimulation therapy. There are several methods to non-invasively measure conductivity of in-vivo tissue at 100-1000 Hz. Magnetic Resonance Electrical Impedance Tomography (MREIT) - the most well established methodology - is based on injecting currents into the human body through skin surface electrodes and recording their induced magnetic field distortion with MRI. A severe disadvantage of MREIT is the risk of pain sensation due to the relatively large injected currents required to achieve sufficient signal to noise ratio (SNR) for a reliable conductivity reconstruction. In this abstract, we investigate a new method to probe electrical properties in-vivo; this method is based on eddy currents induced in tissues by the switching of the readout gradients[2]. In this feasibility study, we report magnetic field distortions caused by induced eddy currents flowing in saline samples by means of simulations and measurements. This should give insight into the physics related to this phenomenon and guide optimization of an MR sequence to measure field distortions.

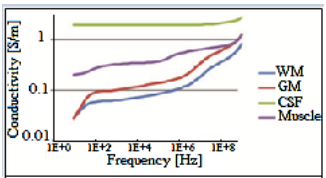

Fig.1: Conductivity values as a function of the frequency.

Materials and Methods: For simulations, four phantoms (Fig. 2a-d) were modelled using GMSH[3], a 3D finite element generator, diameter = 43mm, length = 200mm.

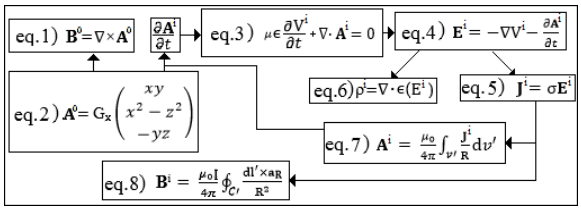

a) Simulation of eddy currents induced by a G_x gradient in phantoms: To calculate the induced electric and magnetic fields we employed a quasi-static (q.s.) approximation. As shown in the scheme on the right, we started by defining the incident magnetic field $\mathbf{B}^0$ arising from the magnetic vector potential $\mathbf{A}^0$ (eq.1, Fig 2e-h). We created $\mathbf{A}^0$ in order to have a gradient field along the x direction (G_x 9.8 mT/m, slew rate 65 T/m/s) and considering the presence of the concomitant fields. Thus, it was possible to calculate the scalar potential V using the Lorentz gauge relation (eq.3). By taking the spatial gradient of the scalar potential, the first order electric field correction can be calculated. Adding this to the incident $\mathbf{E}$ field obtained from the time derivative of $\mathbf{A}^0$, the total first order electric field $\mathbf{E}^1$ is defined (eq.4)[4]. From the electric field $\mathbf{E}^1$, the first order current density $\mathbf{J}^1$ (eq.5, Fig. 2i-l)[5] and the charge accumulation ρ^1 at the boundaries between two regions with different conductivity σ (eq.6, Fig. 2m-p) could be derived.

b) Simulation of induced magnetic field **B** (Fig. 2q-t): Assuming electrostatic conditions, we derived from the induced eddy-current density the induced vector potential $\mathbf{A}^1$ (eq.7) and magnetic field $\mathbf{B}^1$ (eq.8) through the Biot-Savart law. If needed, higher order q.s. corrections A^i, B^i, and E^i can be calculated by a new iteration with the updated magnetic vector potential. In our case, we iterated the loop two times, thus including first and second order corrections.

c) Simulation and measurements of phase accumulation (Fig. 2u-x): For simulations, we calculated the z component of the induced magnetic field $\mathbf{B}^i$, i.e. parallel to B_0. For experimental studies, we built four phantoms (Fig. 2a-d) using cylindrical containers with the same dimensions and conductivity[6] as in the simulations. Two multislice SE data sets were obtained in a 3T MR Scanner (Achieva, Philips Healthcare, Best, The Netherlands) using two opposite readout gradients: G_x 9.8 mT/m, rise time 0.16 ms, slew rate 65 T/m/s, FOV 170×170×55, voxel size 2.5×2.5×2.5 mm. To isolate the phase accumulation due to eddy currents induced by the applied readout gradients, we first subtracted two phase images with reversed readout gradients for all the phantoms[7]. Then we calculated the difference between the results obtained in phantoms with non-zero and zero conductivity making sure that all phantoms were placed at the same position. We employed this method to correct for eddy currents occurring in system components[2].

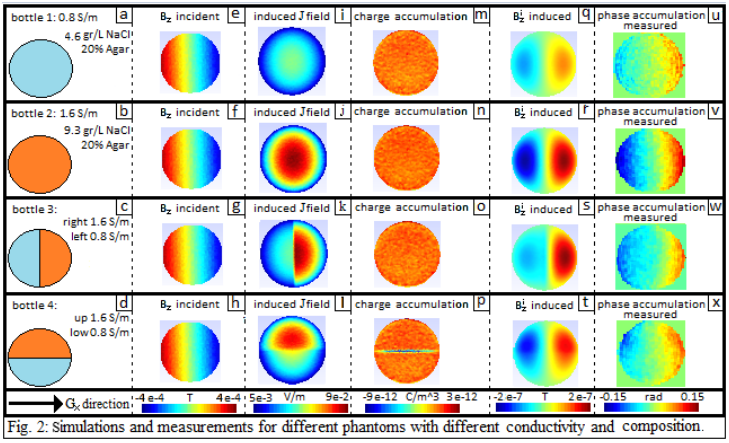

Fig. 2: Simulations and measurements for different phantoms with different conductivity and composition.

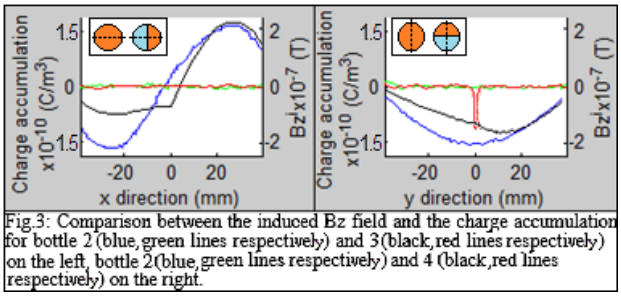

Fig.3: Comparison between the induced Bz field and the charge accumulation for bottle 2 (blue, green lines respectively) and 3 (black, red lines respectively) on the left, bottle 2 (blue, green lines respectively) and 4 (black, red lines respectively) on the right.

Results and Discussion: Starting from a time-varying, linear gradient magnetic field and using the method proposed, we show that it is possible to measure the phase accumulation due to sample eddy currents. Simulations (Fig 2i,j,q,r) and measurements (Fig 2u,v) clearly demonstrate that the induced B_z field and eddy currents are related to the conductivity of the medium. The measurements and simulations correspond reasonably well, except that a small, residual, linear gradient seems to be superimposed on the measurements. In addition the shape of the induced B_z field depends on the orientation of the interface between two different media in relation to the direction of the applied readout gradient, as it is shown in simulations and measurements (Fig 2s,t,w,x and Fig.3). Interestingly, a distinct effect of the interface was observed originating from the charge accumulation at the interface. This is understandable from the continuity equation for current density: if the divergence of **J** is non-zero due to differences in conductivities, there will be charge build up at that location. This accumulation depends also on the orientation of the boundary with respect to the orientation of the linear gradient applied (Fig. 2m-p). This effect was also found in measurements (Fig 2w,x). Finally, it is noteworthy to mention that the phase accumulation does not depend on the rising time but only on the final gradient strength.

Conclusion: In this study, we show that it is possible to measure the phase accumulation caused by the induced B field generated by eddy currents flowing in a sample due to time varying linear imaging gradient fields available on every MRI scanner. By measuring the induced B_z field, we can derive information about the electrical conduction and composition of media, e.g. interfaces and orientation. The fact that the orientation of the interface with respect to the gradient direction influences the induced B_z field is also an important finding. By using many gradient directions, we can potentially derive information about the orientation of interfaces, alike diffusion tensor imaging. Reconstruction of induced currents and even tissue conductivity can be done as in MREIT or using other methods[8].

References: [1] S. Gabriel et al, *Phys. Med. Biol.* 41(11), 1996, 2271-93. [2] van Lier et al, *ISMRM* 20 2012:3467. [3] C. Geuzaine J. F. Remacle, *Int. J. Numer. Math. Engng*. 79 (11), 2009. [4] R. P. Feynman et al, The Feynman Lectures on Physics: Part II, Addison-Wesley, 1964. [5] A. Thielscher et al, *Neuroimage* 54, 2011, 234-243. [6] A. Stogryn, *IEEE Transaction on Microwave Theory and Techniques* 19(8), 1971, 733-6. [7] M. A. Bernstein et al, Handbook of MRI Pulse Sequence, Elsevier, 2004. [8] O. F. Oran et al, *ISMRM* 21 2013:4188.